Pergamon

*Int. J. Solids Structures* Vol. 33, No. 12, pp. 1725–1743, 1996

0020–7683/96 $15.00 + .00

0020–7683(95)00124–7

# THE CRACKED LAP SHEAR SPECIMEN REVISITED—A CLOSED FORM SOLUTION

YEH-HUNG LAI,† M. DWAYNE RAKESTRAW and DAVID A. DILLARD‡

Engineering Science and Mechanics Department, Virginia Polytechnic Institute and State University, Blacksburg, VA 24061-0219, U.S.A.

(*Received* 9 *October* 1994; *in revised form* 15 *May* 1995)

**Abstract**—This paper revisits the cracked lap shear specimen and reports a closed form solution to determine three fracture parameters, the energy release rate, the fracture mode mixity, and the fracture efficiency parameter. The solution is based on a beam-column approach pioneered by Goland and Reissner. Because of the geometrically nonlinear nature of this specimen, it is found that the fracture parameters are functions of five independent nondimensional parameters. The closed form solution reported in this paper provides a simple and useful tool to design the cracked lap shear specimen and to understand the behavior of this test geometry. The results in this paper suggest that to design a specimen with an energy release rate less dependent on the crack length, the adherend thickness should be small compared to the specimen length, and the thicker or stiffer adherend should be used as the strap. For a specimen of unequal adherend thickness, using the thicker adherend as the strap would significantly reduce the likelihood of yielding in the adherend. Compared with the finite element analyses found in the literature, the closed form solution shows good agreement in energy release rates, but less satisfactory agreement in fracture mode mixities. Finally, the closed form solution is used to give a reasonable explanation of anomalous debond behavior in a series of fatigue experiment using the cracked lap shear specimen.

## INTRODUCTION

Shear loaded joints are widely used for adhesively bonded components. Due to the combination of peel and shear stresses, the fracture in a lap shear joint is often a mixed mode problem. The cracked lap shear specimen was originally proposed by Brussat *et al.* (1977) to assess the mixed mode bond fracture strength of the lap shear joint. The cracked lap shear specimen has been used to study adhesive joint debonding (Brussat *et al.*, 1977; Mall *et al.*, 1984; Lin and Liechti, 1987; Schmueser and Johnson, 1990) and composite delamination (Mall *et al.*, 1987; Mall and Yun, 1987). Although the geometry seems simple for testing, it has been found that the results are sensitive to the boundary conditions (Everett and Johnson, 1985; Lin and Liechti, 1987). Furthermore, it was found that to properly determine the mode mixity and the energy release rate, geometrical nonlinearity of the specimen should be considered (Johnson, 1987). Although some analytical solutions have been derived, these solutions are useful for relatively limited cases such as for an infinitely long specimen (Brussat *et al.*, 1977) or for a specimen with the same thickness and material for lap and strap adherends (Edde and Verreman, 1992). The finite element method has been the most widely used tool to obtain the fracture parameters for the cracked lap shear specimens. However, it is difficult to investigate the effects of all the parameters in a cracked lap shear test using the finite element method and the behavior of this test geometry has not been fully understood. Therefore, a comprehensive analytical solution is needed for better analysis and design of the cracked lap shear specimen.

This paper will revisit the cracked lap shear specimen and introduce a new nondimensional closed form solution. The solution is based on a mechanics of materials approach similar to the one used by Goland and Reissner (1944) for a classical single lap shear joint problem. Since the objective of this paper is to obtain the fracture parameters, the elaborated effort for stress distribution in the adhesive layer is not needed. Instead, only

† Present address: Research Labs, Eastman Kodak Company, Rochester, NY 14650-2116, U.S.A.
‡ To whom correspondence should be addressed.

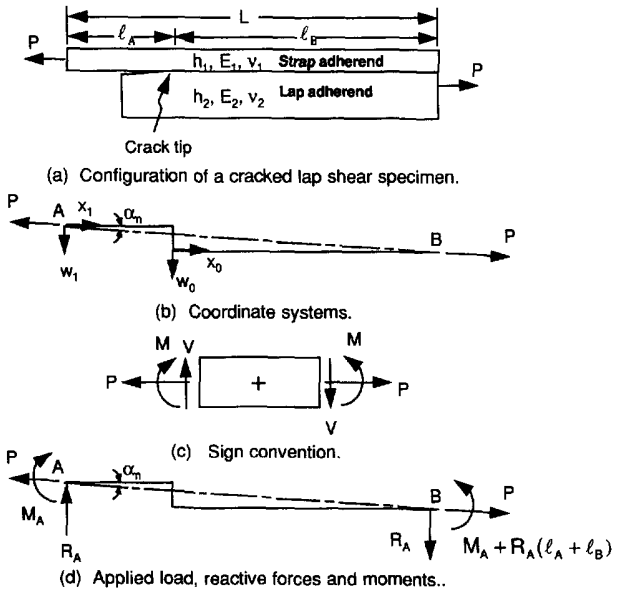


Fig. 1. Illustration of the cracked lap shear configuration.

the bending moment will be solved for and then two fracture parameters, the energy release rate and fracture mode mixity, will be obtained using a recent solution derived by Suo and Hutchinson (1990). In addition, another useful parameter in designing a fracture specimen for adhesive bonds called the fracture efficiency parameter (Lai and Dillard, 1994, 1995) will also be investigated. By designing a cracked lap shear specimen with a higher fracture efficiency parameter, the debonding is more likely to occur without causing adherend yielding, and therefore allows the elastic analysis to be used. Using the closed form solution, the effects of the boundary conditions, specimen dimensions, material properties, and loading conditions on the fracture parameters will be discussed. The closed form solution will also be compared with the results from finite element analyses in the literature. Finally, the solution will be used to understand the anomalous debond behavior in a series of earlier fatigue experiments using cracked lap shear specimens.

## MATHEMATICAL FORMULATIONS

In this section, the deflections and bending moments in a cracked lap shear specimen will be determined using Goland and Reissner's approach (1944) for single lap joints. The cracked lap shear specimen configuration and related parameters are shown in Fig. 1. Following Goland and Reissner's approach, the adhesive layer is assumed to be so thin compared to the adherend that it can be neglected. While the local stresses might change if this layer were included in the analysis, the energy release rate should not be greatly affected. Both ends of the specimen are subjected to a tensile load $P$ and appropriate boundary conditions depending on how the specimen is gripped in the experiment.

Figure 1(b) illustrates the neutral plane of the specimen and the coordinates of the problem. For convenience, two sets of coordinate systems $(x_1, w_1)$ and $(x_0, w_0)$ are introduced for the parts of the specimen to the left and right of the crack tip, respectively; $w_1$ and $w_0$ coordinates represent the transverse deflections of the specimen from the unloaded condition and are positive downward. The sign convention of the bending moment $M$, shear force $V$, and axial force $P$ are shown in Fig. 1(c). In addition to the applied load, $P$, the reaction force, $R_A$, and reaction bending moment, $M_A$, may also exist depending on the types of boundary conditions. The specimen is considered as a plane problem so the forces and moments are averaged over the width of the specimen.

Following Goland and Reissner's approach, we can set $M_1$ and $M_0$ equal to the bending moment at position $x_1$ and $x_0$, each per unit of width, then

$$M_1 = P\left(\alpha_n x_1 - w_1 + \frac{R_A}{P} x_1 + \frac{M_A}{P}\right), \tag{1-1}$$

$$M_0 = P\left[\alpha_n(x_0+\ell_A) - w_0 - \left(\frac{h_1}{2}+h_2-\Delta h_1\right) + \frac{R_A}{P}(x_0+\ell_A) + \frac{M_A}{P}\right], \tag{1-2}$$

where

$$\Delta \text{ is a nondimensional quantity: } \Delta = \frac{1+2\Sigma\eta+\Sigma\eta^2}{2\eta(1+\Sigma\eta)}, \tag{2-1}$$

$$\eta \text{ is the thickness ratio of the strap to lap adherends: } \eta = h_1/h_2, \tag{2-2}$$

$$\Sigma \text{ is the modulus ratio of the strap to lap adherends: } \Sigma = E_1^*/E_2^*, \tag{2-3}$$

$$E_1^* = E_1/(1-\nu_1^2) \quad \text{and} \quad E_2^* = E_2/(1-\nu_2^2) \quad \text{for plane strain cases,} \tag{2-4}$$

$$E_1^* = E_1 \quad \text{and} \quad E_2^* = E_2 \quad \text{for plane stress cases,} \tag{2-5}$$

and $\alpha_n$ represents the angle between the $x_1$ (or $x_0$) coordinates and the line of applied load (AB):

$$\alpha_n = \left(\frac{h_1}{2}+h_2-\Delta h_1\right)\Big/ L. \tag{2-6}$$

Similar to the theory of thin, cylindrically bent plates, the differential equations for the transverse deflections, $w_1$ and $w_0$ can be given by:

$$\frac{d^2 w_1}{dx_1^2} = -\frac{M_1}{D_1} = -\frac{P}{D_1}\left(\alpha_n x_1 - w_1 + \frac{R_A}{P} x_1 + \frac{M_A}{P}\right), \tag{3-1}$$

$$\frac{d^2 w_0}{dx_0^2} = -\frac{M_0}{D_0} = -\frac{P}{D_0}\left[\alpha_n(x_0+\ell_A) - w_0 - \left(\frac{h_1}{2}+h_2-\Delta h_1\right) + \frac{R_A}{P}(x_0+\ell_A) + \frac{M_A}{P}\right], \tag{3-2}$$

where $D_1$ and $D_0$ are the flexural rigidities of the strap adherend at the unbonded section and overlap joint section, respectively. Equations (3) have solutions of:

$$\frac{w_1}{L} = A_1 \cosh(\lambda_1 x_1) + B_1 \sinh(\lambda_1 x_1) + (\alpha_n + \hat{R}_A)\frac{x_1}{L} + \hat{M}_A, \tag{4-1}$$

$$\frac{w_0}{L} = A_0 \cosh(\lambda_0 x_0) + B_0 \sinh(\lambda_0 x_0) + \left[(\alpha_n + \hat{R}_A)\frac{(x_0+\ell_A)}{L} - \alpha_n + \hat{M}_A\right], \tag{4-2}$$

where

$$\lambda_1 = \sqrt{\frac{P}{D_1}}, \quad \lambda_0 = \sqrt{\frac{P}{D_0}} \tag{5}$$

and $\hat{R}_A$ and $\hat{M}_A$ are the nondimensional reaction force and moment which are given by

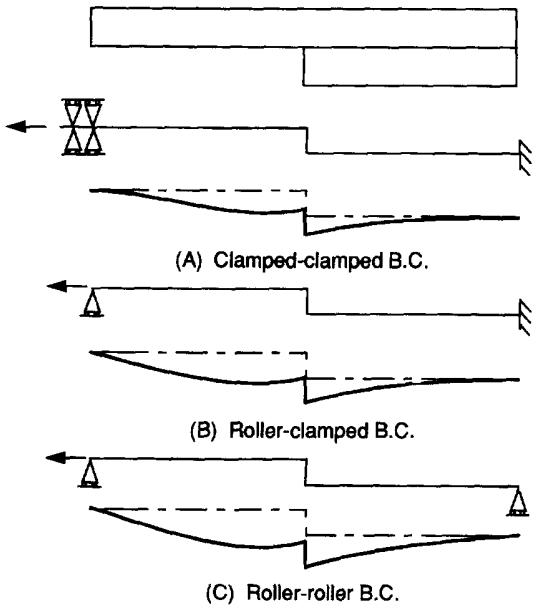


Fig. 2. Three possible configurations of boundary conditions in a cracked lap shear test.

$$\hat{R}_A = \frac{R_A}{P} \tag{6}$$

and

$$\hat{M}_A = \frac{M_A}{PL} \tag{7}$$

respectively.

The unknowns, $A_1$, $B_1$, $A_0$, $B_0$, $\hat{R}_A$ and $\hat{M}_A$ in eqns (4) can be solved by imposing appropriate boundary conditions. Three possible configurations of boundary condition in cracked lap shear test will be investigated in this study (Fig. 2) and are summarized below. The unknown constants determined for the Cases A, B, and C are listed in Appendix A. After the unknown constants are solved, the bending moments in the specimen are readily evaluated. Since the bending moments at $x_1 = \ell_A^-$ and $x_0 = 0^+$ can be directly used to determine the energy release rate and mode mixity as will be discussed in the next section, they are evaluated as:

$$\text{at } x_1 = \ell_A^-, \quad M_1(\ell_A) = PL[-A_1 \cosh(\lambda_1 \ell_A) - B_1 \sinh(\lambda_1 \ell_A)], \tag{8-1}$$

$$\text{at } x_0 = 0^+, \quad M_0(0) = PL\left[-A_2 - \hat{R}_A \frac{\ell_A}{L}\right]. \tag{8-2}$$

Figure 2 also shows the typical deformed shape of the neutral axis for different boundary conditions. The thickness and transverse deflection have been magnified by 10 and 150 times, respectively.

*Case A. Clamped–clamped configuration*

This case is representative of typical testing in fixed grips of a universal test machine. In this case, six boundary conditions can be found by solving for the six unknown constants, $A_1$, $B_1$, $A_0$, $B_0$, $\hat{R}_A$, and $\hat{M}_A$:

$$w_1(0)=0;\quad \left.\frac{dw_1}{dx_1}\right|_{x_1=0}=0;\quad w_1(\ell_A)=w_0(0);\quad \left.\frac{dw_1}{dx_1}\right|_{x_1=\ell_A}=\left.\frac{dw_0}{dx_0}\right|_{x_0=0};$$

$$w_0(\ell_B)=0;\quad \left.\frac{dw_0}{dx_0}\right|_{x_0=\ell_B}=0. \tag{9}$$

*Case B. Roller–clamped configuration*

This configuration is frequently cited in the literature (Johnson, 1987; Dattaguru *et al.*, 1984; Mall and Sun, 1987). In this case, the reaction moment $M_A$ is equal to zero and five boundary conditions can be found by solving for the five unknown constants, $A_1$, $B_1$, $A_0$, $B_0$, and $\hat{R}_A$:

$$w_1(0)=0;\quad w_1(\ell_A)=w_0(0);\quad \left.\frac{dw_1}{dx_1}\right|_{x_1=\ell_A}=\left.\frac{dw_0}{dx_0}\right|_{x_0=0};\quad w_0(\ell_B)=0;\quad \left.\frac{dw_0}{dx_0}\right|_{x_0=\ell_B}=0. \tag{10}$$

*Case C. Roller–roller configuration*

This configuration is equivalent to half of the single lap shear joint problem solved by Goland and Reissner (1944). Four boundary conditions are found in this case in which the reaction force $R_A$ and moment $M_A$ are equal to zero. The boundary conditions are:

$$w_1(0)=0;\quad w_1(\ell_A)=w_0(0);\quad \left.\frac{dw_1}{dx_1}\right|_{x_1=\ell_A}=\left.\frac{dw_0}{dx_0}\right|_{x_0=0};\quad w_0(\ell_B)=0. \tag{11}$$

## ENERGY RELEASE RATE AND MODE MIXITY

Using the energy release rate and stress intensity factors derived by Suo and Hutchinson (1990) for an interfacial crack in a bilayer with each layer being homogeneous, isotropic, and linearly elastic, these fracture parameters in a cracked lap shear specimen can be determined.

The energy release rate is given by

$$G=\frac{1}{2E_1^*}\left(\frac{P^2}{h_1}+12\frac{M_1^2(\ell_A)}{h_1^3}\right)+\frac{1}{2E_2^*}\left(-\frac{P^2}{Ah_1}-\frac{M_0^2(0)}{Ih_1^3}\right), \tag{12}$$

where

$$A=\frac{1}{\eta}+\Sigma, \tag{13}$$

and

$$I=\Sigma\left[\left(\Delta-\frac{1}{\eta}\right)^2-\left(\Delta-\frac{1}{\eta}\right)+\frac{1}{3}\right]+\frac{\Delta}{\eta}\left(\Delta-\frac{1}{\eta}\right)+\frac{1}{3\eta^3}. \tag{14}$$

The complex stress intensity factor is given by

$$K = K_I + iK_{II}$$

$$= h_1^{-i\varepsilon}\left(\frac{1-\alpha}{1+\beta^2}\right)^{1/2}\left(\frac{-P+C_1P-C_2M_0(0)/h_1}{\sqrt{2h_1U}} - ie^{i\gamma}\frac{M_1(\ell_A)-C_3M_0(0)}{\sqrt{2h_1^3V}}\right)e^{i\omega} \quad (15)$$

where $\alpha$ and $\beta$ are Dundur's elastic mismatch parameters which are given by

$$\alpha = \frac{E_1^*-E_2^*}{E_1^*+E_2^*} \quad \text{and} \quad \beta = \frac{1}{2}\frac{E_1(1-2\nu_2)/(1+\nu_1)-E_2(1-2\nu_1)/(1+\nu_2)}{E_1(1-\nu_2)/(1+\nu_1)+E_2(1-\nu_1)/(1+\nu_2)}, \quad (16)$$

$\varepsilon$ is a bimaterial constant:

$$\varepsilon = \frac{1}{2\pi}\ln\left(\frac{1-\beta}{1+\beta}\right), \quad (17)$$

$C_1$, $C_2$, $C_3$, $U$, $V$ and $\gamma$ are geometric factors and are given by

$$C_1 = \frac{\Sigma}{A}, \quad C_2 = \frac{\Sigma}{I}\left(\frac{1}{\eta}+\frac{1}{2}-\Delta\right), \quad \text{and} \quad C_3 = \frac{\Sigma}{12I}, \quad (18\text{-}1)$$

and by

$$U = \frac{1}{1+\Sigma\eta(4+6\eta+3\eta^2)}, \quad V = \frac{1}{12(1+\Sigma\eta^3)}, \quad \text{and} \quad \sin\gamma = 6\Sigma\eta^2(1+\eta)\sqrt{UV}, \quad (18\text{-}2)$$

and the angle $\omega$ is a function of the Dundur's parameters and adherend thickness ratio, $\eta$. The table of $\omega$ can be found in Suo and Hutchinson (1990).

The mode mixity can be conveniently represented by the phase angle which is given by

$$\psi = \tan^{-1}\left(\frac{K_{II}}{K_I}\right). \quad (19)$$

When the phase angle is negative, the crack would tend to grow toward the adhesive/strap interface. Alternately, when the phase angle is positive, the crack would tend to grow toward the adhesive/lap interface.

It should be noted that the relations in eqns (12) and (15) are based on the assumption that the thickness of the adhesive layer is very small compared with in-plane dimensions of the specimen and is negligible. Therefore the energy release rate and stress intensity factors in eqns (12) and (15) are global quantities. Although it can be proved that the global energy release rate is equal to the local energy release rate at the crack tip using a simple energy argument or application of the $J$-integral, the global stress intensity factors are not always equal to the local stress intensity factors at the crack tip. The relation between the global and local stress intensity factors can be found in Fleck *et al.* (1991). Based on the study by Fleck *et al.* the global phase angle obtained in this paper is equal to the local phase angle of a crack locating at the middle of the bond line when both adherends are made of the same material. One should be able to follow the procedure by Fleck *et al.* to obtain the phase angle of cracks located at various locations through the bond thickness.

As seen in Appendix A, the debond problem in a cracked lap shear specimen can be described by five nondimensional parameters: nondimensional axial load, $\hat{P} = \sqrt{P/E_1^*(h_1+h_2)}$; nondimensional crack tip position, $q = \ell_A/L$; nondimensional strap

thickness, $\kappa = h_1/L$; nondimensional adherend thickness ratio, $\eta = h_1/h_2$; and nondimensional adherend modulus ratio, $\Sigma = E_1^*/E_2^*$. With the above five nondimensional quantities, the energy release rate can be rewritten as:

$$G = \frac{P^2}{2(E_1^*+E_2^*)(h_1+h_2)}\left\{\left(1+\frac{1}{\Sigma}\right)\left[\left(1+\frac{1}{\eta}\right)+12\hat{M}_1^2\left(1+\frac{1}{\eta}\right)^3\right]-(1+\Sigma)\left[\frac{(1+1/\eta)}{A}+\hat{M}_0^2\frac{(1+1/\eta)^3}{I}\right]\right\}, \quad (20)$$

where $\hat{M}_1$ and $\hat{M}_0$ are the nondimensional bending moments which are given by

$$\hat{M}_1 = \frac{M_1(\ell_A)}{P(h_1+h_2)} \quad \text{and} \quad \hat{M}_0 = \frac{M_0(0)}{P(h_1+h_2)}. \quad (21)$$

The quantity $\hat{G}$ is called the nondimensional energy release rate and is given by:

$$\hat{G} = G\frac{(E_1^*+E_2^*)(h_1+h_2)}{P^2}. \quad (22)$$

Equation (20) can be used for the cracked lap shear specimen subjected to various boundary conditions. The effects of the boundary conditions on the energy release rate and mode mixity will be passed through the bending moments, $\hat{M}_1$ and $\hat{M}_0$.

For comparison purposes, it is interesting to note that the total energy release rate obtained by Brussat *et al.* (1977) for an infinitely long specimen is given by

$$G = \frac{P^2}{2E_1^*h_1}\left(1-\frac{E_1^*h_1}{E_1^*h_1+E_2^*h_2}\right) = \frac{P^2}{2(E_1^*+E_2^*)(h_1+h_2)}\left(1+\frac{1}{\Sigma}\right)\left(1+\frac{1}{\eta}\right)\left(1-\frac{\Sigma\eta}{\Sigma\eta+1}\right). \quad (23)$$

Note that energy release rate obtained from eqn (23), which can also be derived from eqn (20) when $\ell_A$ and $\ell_B$ approach infinity, is independent of the crack length. It can be used as a limiting case for specimens of cases A, B, and C.

Since the solution reported in this paper is based on the Goland and Reissner approach and Suo and Hutchinson's solution, it is conceivable that the solution may deteriorate as the adhesive thickness is no longer small compared to the adherend thicknesses or as the adhesive layer becomes relatively flexible compared to the adherend. In a comprehensive study by Tsai and Morton (1994) using nonlinear finite element analysis, it was found that using Goland and Reissner's solution in predicting the bending moment $M_1(\ell_A)$ in the single lap shear joint induced less than 10% of error when the adhesive thickness was less than 15% of the adherend thickness, or less than 20% of error when the adhesive modulus was larger than 0.8% of the adherend modulus. Since the contribution of bending moment to the total energy release rate in a cracked lap shear specimen is typically within 25%, the use of Goland and Reissner's approach in predicting the energy release rate would induce much less error than in the prediction of $M_1(\ell_A)$.

## FRACTURE EFFICIENCY FOR CRACKED LAP SHEAR SPECIMENS

Since the current analysis is based on the assumption that the adherends are loaded within the elastic range, the solution would become invalid if one or both of the adherend yielded. Recently, Lai and Dillard (1994, 1995) proposed a concept called the fracture efficiency to evaluate the performance of fracture tests for measuring the bond fracture

strength of adhesive joints. A test with a high fracture efficiency may be used to debond the specimen without causing yielding in the adherend, and therefore allows one to determine the bond fracture strength using an elastic analysis method. The fracture efficiency is evaluated based on a simple quantity called the fracture efficiency parameter, which is defined as

$$T_e = \frac{G}{\sigma_{max}^2}, \tag{24}$$

where $\sigma_{max}$ is the maximum non-singular stress in the adherend, which is the sum of the bending stress and axial stress in the adherend of the cracked lap shear specimen. The fracture efficiency parameter can also be expressed as

$$T_e = \frac{C_e \lambda^*}{E^*}, \tag{25}$$

where $\lambda^*$ is a characteristic length, $E^*$ is a characteristic modulus, and $C_e$ is a non-dimensional parameter. In a cracked lap shear test, the characteristic length, $\lambda^*$, is equal to $(h_1+h_2)$ and the characteristic modulus, $E^*$, is equal to $(E_1^*+E_2^*)$.

## RESULTS AND DISCUSSIONS

Although five nondimensional parameters are found in the solution, the authors do not attempt to explore every case with all the possible combinations of five parameters. Instead, typical parameters found in the literature and in the experiments will be used. Fortunately, the solution has been nondimensionalized so that the results can be used in many other cases as well.

Figure 3 illustrates the nondimensional energy release rate versus the nondimensional position of the crack tip for various nondimensional strap thicknesses. The results of three sets of boundary conditions are plotted in the same figure. In this case, the strap and lap adherends are assumed to have the same thickness and material properties. The non-dimensional applied load is taken as 0.01, which is similar to those found in the literature. The cases with clamped–clamped, roller–clamped and roller–roller boundary conditions are

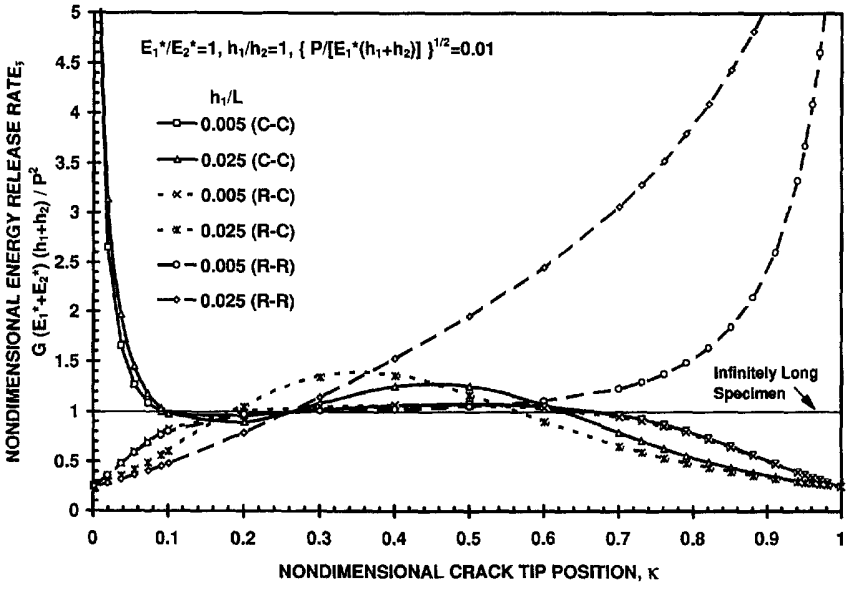


Fig. 3. Nondimensional energy release rate versus nondimensional position of the crack tip for various nondimensional strap thicknesses.

denoted as (C-C), (R-C), and (R-R) in the key. Typical nondimensional strap thicknesses of 0.005 and 0.025 are used, corresponding to a specimen of 305 mm (12 inches) in length and 1.59 mm (1/16 inch) in the strap adherend thickness and a specimen of 254 mm (10 inches) in length and 6.35 mm (1/4 inch) in thickness, respectively. These dimensions are also similar to those found in the literature. Three stages of crack growth can be seen in this figure. The first is when the crack tip moves away from the left end of the strap to a nondimensional position of about 0.2. The second stage is when the crack tip moves from a nondimensional position of about 0.2 to 0.7. The last stage is when the crack moves from 0.7 toward the right end of the specimen. In the first stage, the energy release rates in all cases change significantly. If the initial cracks are growing within this region, the specimens are expected to have a significant change in debonding rate. In the second stage, the energy release rates for the three cases of nondimensional strap thickness of 0.005 are nearly constant. The value is approximately equal to that found for an infinitely long specimen using eqn (23). These results suggest that as the nondimensional strap thickness is reduced further, the strain energy release will converge toward this value and the specimen can have a larger testing window with only a small change in the energy release rate. In the same region, the cases of clamped–clamped and roller–clamped boundary conditions with a nondimensional strap thickness of 0.025 have about a 25% variation of energy release rate. Larger variation in energy release rate during the debonding process is expected if the nondimensional strap thickness is increased more. In the last stage, a significant change in energy release rate is seen again for all cases.

From the results in Fig. 3, the energy release rate in the roller–roller case is the most sensitive to the nondimensional strap thickness, while the clamped–clamped case is the least sensitive. The results suggest that the clamped-clamped configuration is more applicable over a wider range of nondimensional strap adherend thickness. Fortunately, this is also most frequently encountered in experimental test fixtures. The effects of the applied load and material modulus can also be investigated through Fig. 3 since decreasing the nondimensional strap thickness has the same effect as decreasing the modulus or increasing the applied load as can be seen in the nondimensional form of the applied load in eqn (A.1). The results suggest that by decreasing the nondimensional strap thickness, modulus, or increasing the applied load, the effects of the boundary conditions would be less significant and the specimen would behave more like the infinitely long specimen.

Figure 4 illustrates the phase angle versus the nondimensional crack tip position for specimens with the same parameters found in the discussions of Fig. 3. The phase angle

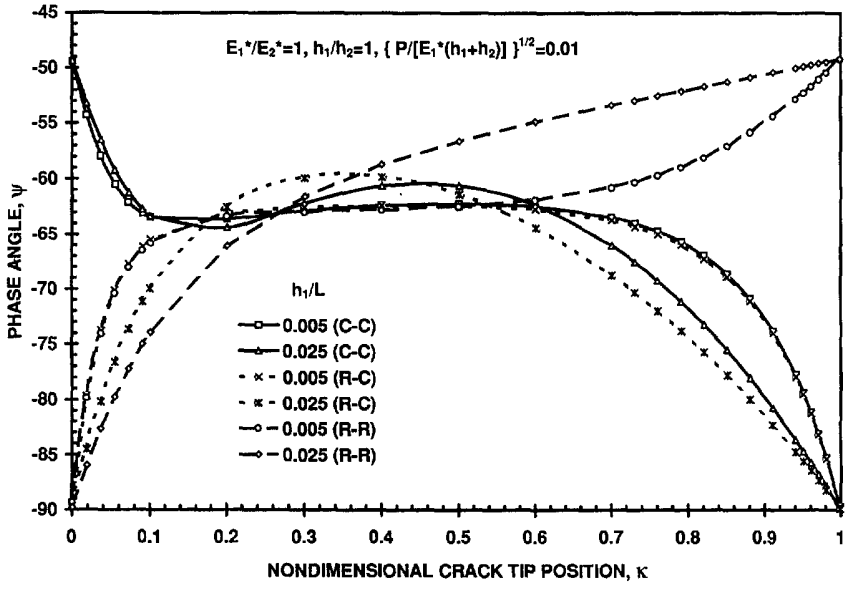


Fig. 4. Phase angle versus the nondimensional crack tip position for various nondimensional strap thicknesses.

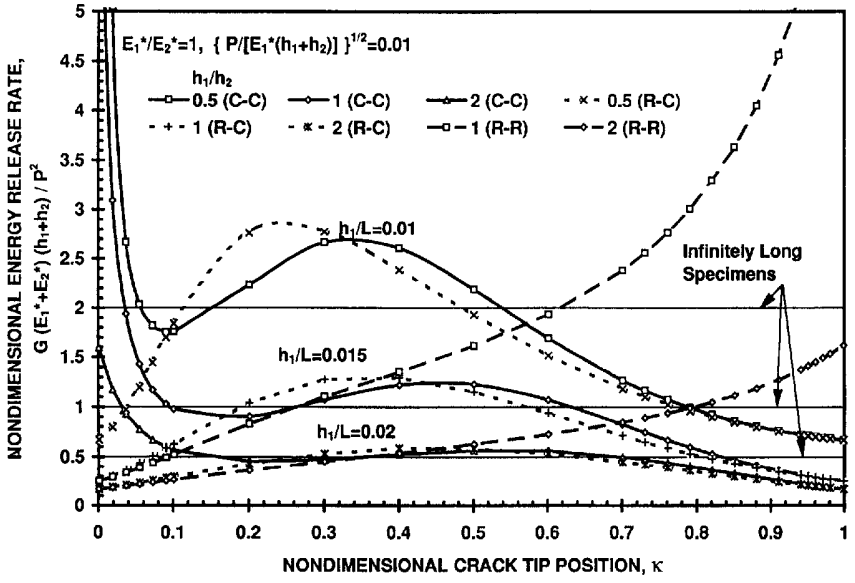


Fig. 5. Nondimensional energy release rate versus nondimensional crack tip position for cracked lap shear specimens with various thickness ratios and nondimensional strap thicknesses.

trends parallel the discussion of the energy release rate. It is seen that the crack tip is predominately loaded in mode II. The negative phase angle suggests that the crack would tend to grow toward the adhesive/strap interface.

Figures 5 and 6 show the nondimensional energy release rate and nondimensional fracture efficiency parameter versus the nondimensional crack tip position, respectively, for cracked lap shear specimens with various thickness ratios and nondimensional strap thickness. For comparison purposes, three thickness ratios are chosen as 2, 1 and 0.5. The same material is used in the strap and lap adherends. In order to compare the magnitudes of the energy release rate under the same applied load with different thickness ratios, the sum of the strap and lap adherend thickness is taken as a constant. The specimen lengths for all cases are also the same. The nondimensional strap thicknesses for different thickness

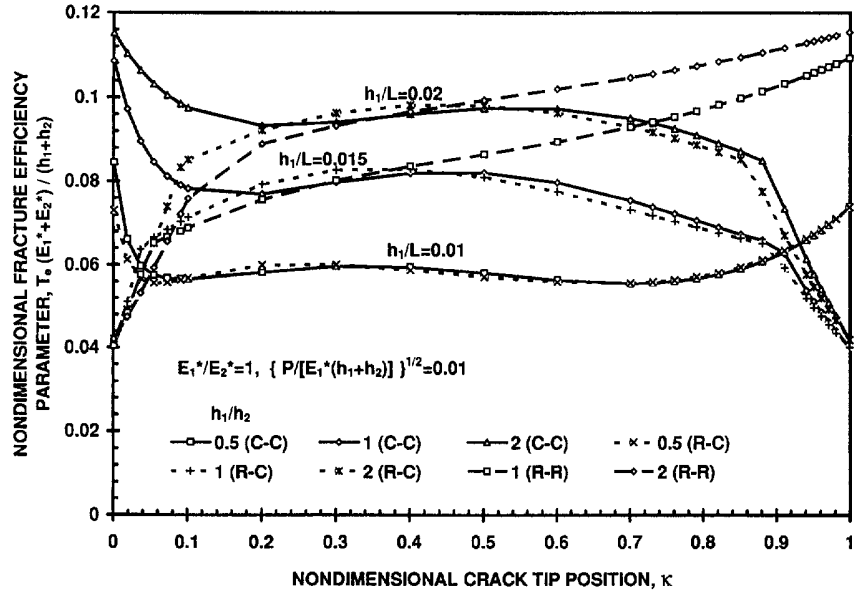


Fig. 6. Nondimensional fracture efficiency parameter versus nondimensional crack tip position for cracked lap shear specimens with various thickness ratios and nondimensional strap thickness.

ratios are adjusted accordingly. The nondimensional applied load is chosen as 0.01. Although only three cases are examined in Figs 5 and 6, the results represent trends for a wider range of adherend thickness ratio.

In Fig. 5, it is seen that for all boundary conditions in the main testing region where the nondimensional crack tip position is between 0.2 and 0.7, the thickness ratio of 0.5 produces the highest energy release rate and the thickness ratio of 2 has the lowest of the three cases examined. However, it is more important to see that the thickness ratio of 0.5 has more variation in the energy release rate as the crack grows while the thickness ratio of 2 remains nearly constant. Therefore, from the viewpoint of the experiment, it is preferred to use the strap thicker than the lap in order to have a stable crack growing test. In spite of the smaller energy release rate for the specimens with higher thickness ratios, one could always increase the axial load to increase the energy release rate while maintaining the stable crack growing advantage using the higher thickness ratio specimens. Although increasing the load will increase the adherend stress and may cause the specimen to yield, whether the specimens with different thickness ratios will yield before debonding should be investigated through the fracture efficiency parameter as plotted in Fig. 6.

In Fig. 5, the results obtained from eqn (23) for an infinitely long specimen are also plotted, which have values of 2, 1, and 0.5 for the cases of thickness ratio equal to 0.5, 1, and 2, respectively. These three straight lines can serve as the limiting energy release rates when the specimens are subjected to a very large load, or have very compliant materials in the adherends, or have very thin adherends, or are very long.

The comparison of the nondimensional fracture efficiency parameters,

$$C_e = T_e \frac{E_1^* + E_2^*}{h_1 + h_2},$$

for different adherend thickness ratios are seen in Fig. 6. The maximum non-singular stress is found to locate at either side of the crack tip. In general, it is located at the inner surface at the debonded side of the strap adherend, although it can be located at the bonded side of the specimen. The kink in the curve of nondimensional adherend thickness of 2 in the clamped–clamped case represents the maximum non-singular stress switching sides. From Fig. 6, it is interesting to note that although a specimen with a smaller adherend thickness ratio produces higher energy release rates, it actually has a smaller fracture efficiency parameter due to the higher adherend stress. Therefore, the specimens with higher adherend thickness ratio not only have the advantage of more stable growth but also have the advantage of higher fracture efficiency. It should be noted that unlike a linear system in which the fracture efficiency parameter is independent of applied load, the fracture efficiency parameter of the cracked lap shear specimens depends on the applied load through the dependence of the nondimensional applied load. However, this dependence is much weaker than the dependence of the energy release rate or adherend stresses on the applied load.

Figure 7 illustrates the nondimensional fracture efficiency parameter versus adherend thickness ratio for an infinitely long cracked lap shear specimen. The nondimensional fracture efficiency parameter increases as the adherend thickness ratio increases and after reaching a maximum value of 0.097 at an adherend ratio of about 3, it decreases. The result suggests that if one needs to test a cracked lap shear specimen with unequal thickness in the adherends, using the thicker adherend as the strap would be more likely to prevent yielding in the adherend and is a better specimen design. Since the fracture efficiency parameter is less sensitive to the crack tip position than the energy release rate, as is seen in the case of 0.01 nondimensional strap thickness in Figs 5 and 6, the trend in Fig. 7 is believed to be applicable to finite specimen length cases.

Figure 8 illustrates the nondimensional energy release rate versus nondimensional position of the crack tip for various adherend modulus ratios. Similar results to those in Fig. 5 are seen in this figure. More constant energy release rates can be obtained by using the stiffer material for the strap adherend. The results are consistent with those of Fig. 6 in

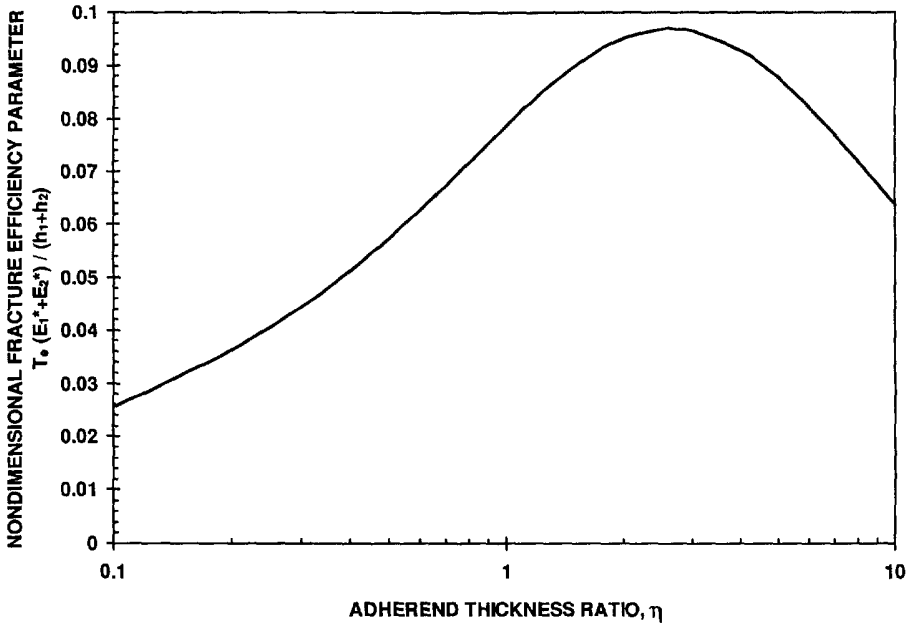


Fig. 7. Nondimensional fracture efficiency parameter versus adherend thickness ratio for infinitely long cracked lap shear specimens.

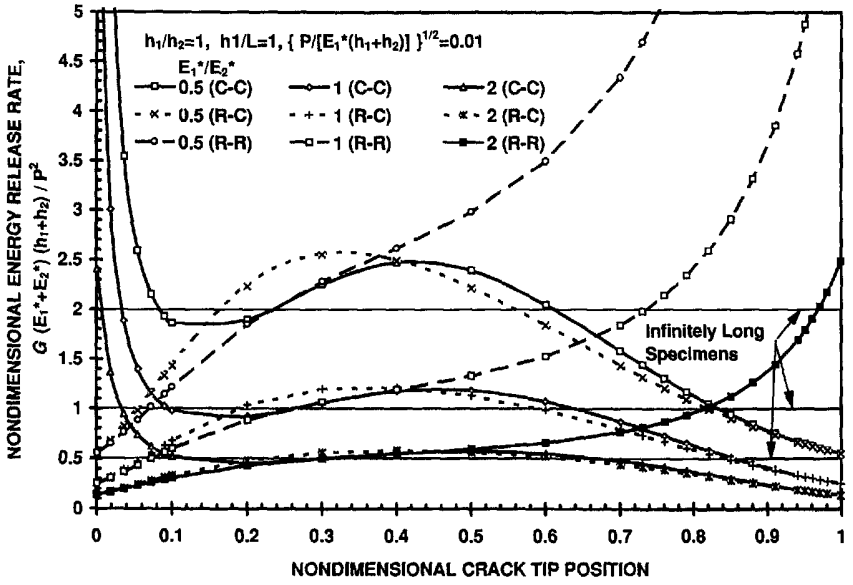


Fig. 8. Nondimensional energy release rate versus nondimensional position of the crack tip for various adherend modulus ratios.

which the larger rigidity in the strap adherend results in more constant but smaller energy release rates.

*Comparison between the closed-form solutions and finite element analyses*

In order to examine the accuracy of the closed-form solutions derived in this study, numerous results of nonlinear finite element analysis were taken from the literature to compare with the closed-form solutions. These problems adapted from the literature are listed in Appendix B.

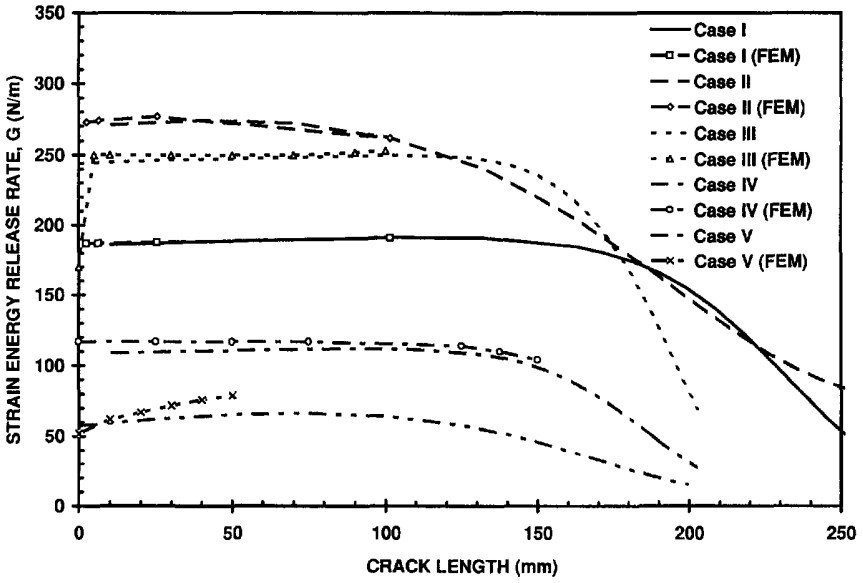


Fig. 9. Comparison of energy release rates between the closed-form solution and various finite element analyses.

The comparison of energy release rates between the closed form solution and various finite element analyses is shown in Fig. 9. Very good agreement is seen for all cases with roller–clamped boundary conditions. The deviation in the clamped–clamped case is larger, but still less than 17%. Since only one case of clamped–clamped boundary conditions was found in the literature, it is not clear why the error is larger than those found in the roller–clamped cases. Although the closed form solution gives the possible energy release rates as the crack grows from zero crack length to the full length of the lap, the longest crack length in all of the finite element analyses is less than 60% of the lap length. In Cases III and IV, the material properties in the fiber direction are used in eqn (12) to determine the energy release rates, since the majority of strain energy is due to the stresses in the fiber direction of the composite adherends. Although eqn (12) is based on the assumption that the adherends are made of isotropic materials, the results suggest that it is also a good approximation for the composite materials study as long as the material properties in the fiber direction are used.

Figure 10 shows the phase angle comparison between the analytical and finite element analysis. It should be noted that the phase angle obtained from eqns (15) and (19) is the global phase angle which is based on the assumption of a negligible adhesive layer. Since the adhesive layers were modeled in the finite element analysis, the phase angle from the finite element analysis could be viewed as the local phase angle. Of all five cases, the phase angles are within 10% of deviation when both adherends are made of the same materials. In Case III, the deviation is 20%, which could be due to the fact that strap and lap adherends are made of different materials. Relatively large deviation (10%) is also seen in Case II in which the strap and lap adherends have unequal thickness. Why the agreement in the phase angle in this case is not as good as in the energy release rate is not fully understood.

In the fatigue problems of the cracked lap shear specimens, whether total energy release rate or the individual fracture mode correlates better with the crack growth rate is still disputable. Although many reported that total energy release rate had a better correlation to the crack growth rate (Mall *et al.*, 1984, 1987; Lin and Liechti, 1987), others found that the crack growth rate correlated better with mode I energy release rate (Dattaguru *et al.*, 1984). It should be noted that, from the study by Fleck *et al.* (1991), the phase angle can have a variation of at least 25° from the adhesive/lap interface to the adhesive/strap interface. Therefore, the phase angle obtained from this paper should be converted into the

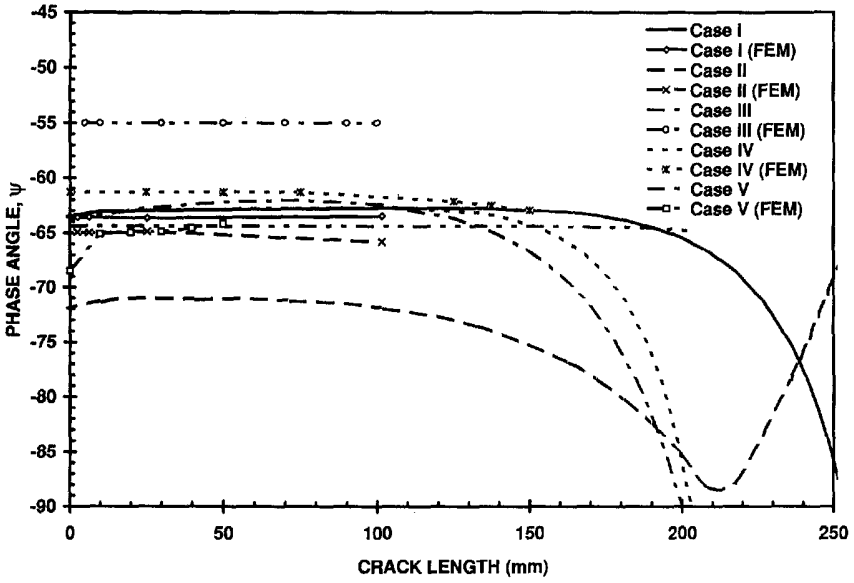


Fig. 10. Phase angle comparison between the analytical and finite element analysis.

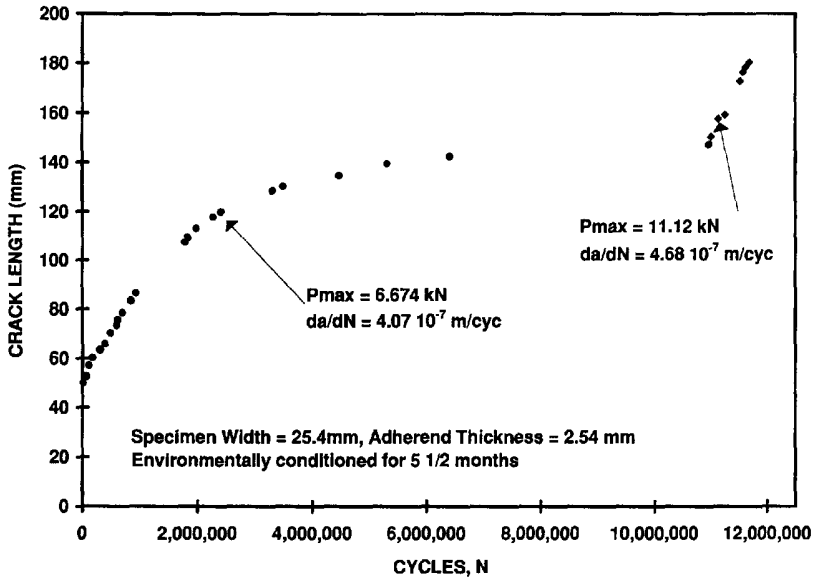


Fig. 11. A typical fatigue crack growth history using a cracked lap shear specimen.

local phase angle depending on the location of the crack and the material properties of the adherends.

*Explanation of anomalous fatigue crack growth data*

In the discussions for Figs 11 and 12, the closed form solution will be used to understand an anomalous crack growth behavior of cracked lap shear specimens used in a fatigue study prior to the current analytical investigation.

A typical crack growth history of a series of fatigue tests using the cracked lap shear specimens is seen in Fig. 11. The strap and lap adherends were made of steel and had a thickness of 2.54 mm and a width of 25.4 mm. The adhesive was an epoxy. The specimen had been conditioned for five and a half months in an environmentally controlled chamber with 99% relative humidity and 60°C. The specimen was clamped at both ends using hydraulic grips and was subjected to a 10Hz cyclic load between 6.674 and 0.667 kN using

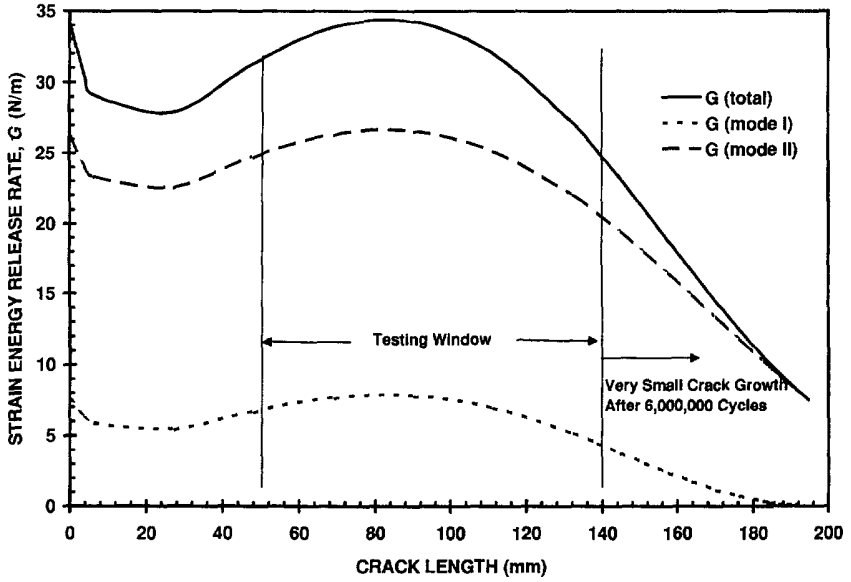


Fig. 12. Energy release rate versus crack length for the specimen discussed in Fig. 11.

an MTS load frame. The initial crack length measured from the edge of the lap adherend to the crack tip was 50 mm. The total specimen length between the grips was 210 mm. The length of the lap adherend less the gripped length was 195 mm. The crack was successfully initiated and grew for about 90 mm. However, the debonding rate decreased as the crack grew longer and nearly stopped at a crack length of 140 mm after about six-million cycles. After another five million cycles, the specimen showed very little crack growth.

Figure 12 illustrates the energy release rate versus crack length. It is seen that the energy release rate increases slightly and then decreases in the test windows found in the fatigue test. When the crack first starts to grow, the total energy release rate is about 31 N $m^{-1}$. When the crack stops growing, the total energy release rate has dropped below 25 N $m^{-1}$ which is a 24% decrease from the initial value. By examining the phase angle, it is found that the global phase angle has changed from $-63°$ to $-65°$, which may not be significant enough to stop the crack growth. Therefore, it is suspected that the reason the crack stopped is because the applied energy release rate dropped below a possible threshold value, 25 N $m^{-1}$. Indeed, after the maximum load was increased from 6.674 to 11.12 kN, the crack resumed growing, as seen in Fig. 11.

## CONCLUSIONS

This paper reported a closed form, nondimensional, geometrically nonlinear solution for cracked lap shear specimens with three sets of possible boundary conditions. The solution was derived based on a beam-column approach similar to that pioneered by Goland and Reissner. The fracture parameters such as the energy release rate and phase angle were emphasized although the stress distribution along the bondline could have been obtained. Besides boundary conditions, it was found that the fracture parameters are functions of five independent nondimensional parameters. The number of independent parameters suggests that it is almost impossible to fully understand the fracture behavior of the cracked lap shear specimen using the geometrically nonlinear finite element method. In view of the sensitivity of energy release rates to the crack growth, the use of clamped–clamped boundary conditions is recommended. In order to obtain a more constant energy release rate test, the specimens should be designed so that the adherend thickness is small compared with the specimen length and the thicker or stiffer adherend should be used as the strap adherend.

The study of the fracture efficiency parameter in an unequal adherend thickness specimen shows that although the specimen using thinner adherend as the strap produces higher energy release rates at a lower load, it would induce higher bending stresses near the debond front and would be more likely to induce yielding in the adherend. It is recommended that when yielding in the adherend is the major concern, one should use the thicker adherend as the strap to achieve a higher fracture efficiency parameter and, therefore, to reduce the likelihood of adherend yielding. This case also served as an excellent example of how the fracture efficiency parameter can be used to design better specimens.

The fracture parameters obtained from the closed form solution were compared with those from the finite element analysis found in the literature. Very good agreement was found for all roller–clamped cases. Good agreement in the phase angle was also found except for the case with different material properties. The closed form solution also gave a reasonable explanation of why the crack growth slowed down significantly after the crack tip reached a specific position in a series of fatigue tests. The slowing down of the debond growth is from the decreasing of the energy release rate as the debond length increases. It is believed that this type of problem could have been avoided by a better design of the specimen dimensions using the solution presented in this paper.

*Acknowledgments*—The authors would like to acknowledge the financial support of the National Science Foundation's Science and Technology Center on High Performance Polymeric Adhesives and Composites at Virginia Tech (Contract DMR 9120004), the Center for Adhesive and Sealant Science at Virginia Tech, and Dow Chemical Company.

## REFERENCES

Brussat, T. R., Chiu, S. T. and Mostovoy, S. (1977). *Fracture Mechanics for Structural Adhesive Bonds*, AFNL-TR-77-163, Air Force Materials Laboratory, Wright-Patterson AFB, Ohio.

Dattaguru, B., Everett, R. A., Jr., Whitcomb, J. D. and Johnson, W. S. (1984). Geometrically nonlinear analysis of adhesively bonded joints. *J. Engng Mater. Technol.* **106,** 59–65.

Edde, F. and Verreman, Y. (1992). On the fracture parameters in a clamped cracked lap shear adhesive joint. *Int. J. Adhesion Adhesives* **12(1),** 43–48.

Everett, R. A. Jr. and Johnson, W. S. (1985). Repeatability of mixed-mode adhesive bonding. In *Delamination and Debonding of Materials* (Edited by W. S. Johnson), STP 876, 267–281. American Society for Testing and Materials.

Fleck, N. A., Hutchinson, J. W. and Suo, Z. (1991). Crack path selection in a brittle adhesive layer. *Int. J. Solids Structures* **27(13),** 1683–1703.

Goland, M. and Reissner, E. (1944). The stresses in cemented joints. *J. Appl. Mech.* **66,** A-17.

Johnson, W. S. (1987). Stress analysis of the cracked lap shear specimen: an ASTM round robin. *ASTM J. Testing and Evaluation* **15,** 303–324.

Lai, Y. H. and Dillard, D. A. (1994). A study of fracture efficiency parameter of blister tests for films and coatings. *J. Adhesion Sci. Technol.* **8,** 663–678.

Lai, Y. H. and Dillard, D. A. (1995). Using the fracture efficiency to compare adhesion tests. *Int. J. Solids Structures* (in revision).

Lin, C. and Liechti, K. M. (1987). Similarity concepts in the fatigue fracture of adhesively bonded joints. *J. Adhesion* **21,** 1–24.

Mall, S., Johnson, W. S. and Everett, R. A. Jr. (1984). Cyclic debonding of adhesively bonded composites. In *Adhesive Joints: their Formation Characteristics and Testing* (Edited by K. L. Mittal), pp. 639–658. Plenum, New York.

Mall, S., Rezaizadeh, M. A. and Gurumurthy, R. (1987). Interaction of mixed-mode loading on cyclic debonding in adhesively bonded composite joints. *J. Engng Mater. Technol. (Trans. ASME)* **109,** 17–21.

Mall, S. and Yun, K. T. (1987). Effect of adhesive ductility on cyclic debond mechanisms in composite-to-composite bonded joints. *J. Adhesion* **23,** 215–231.

Schmueser, D. W. and Johnson, N. L. (1990). Effect of bondline thickness on mixed-mode debonding of adhesive joints to electroprimed steel surfaces. *J. Adhesion* **32,** 171–191.

Suo, Z. and Hutchinson, J. W. (1990). Interface crack between two elastic layers. *Int. J. Fracture* **43,** 1–18.

Tsai, M. Y and Morton, J. (1994). An evaluation of analytical and numerical solutions to the single-lap joint. *Int. J. Solids Structures* **31,** 2537–2563.

## APPENDIX A

The unknown constants in eqn (4) can be easily solved by linear algebra. After careful examination, it is found that all the parameters can be expressed by the following five nondimensional quantities:

nondimensional applied load:

$$\hat{P} = \sqrt{\frac{P}{E_1^*(h_1+h_2)}}, \tag{A.1}$$

nondimensional crack tip position:

$$q = \frac{\ell_A}{L}, \tag{A.2}$$

nondimensional strap thickness:

$$\kappa = \frac{h_1}{L}, \tag{A.3}$$

adherend thickness ratio:

$$\eta = \frac{h_1}{h_2}, \tag{A.4}$$

and adherend modulus ratio:

$$\Sigma = \frac{E_1^*}{E_2^*}. \tag{A.5}$$

To simplify the expressions of the unknown constants, the following nondimensional notations are introduced.

$$a_1 = \sinh(\lambda_1 \ell_A) = \sinh\left(\frac{q}{\kappa}\hat{P}\sqrt{12(1+1/\eta)}\right), \tag{A.6}$$

$$a_2 = \frac{\lambda_1}{\lambda_0} = 2\sqrt{3I/\Sigma}, \tag{A.7}$$

$$a_3 = \cosh(\lambda_1 \ell_A) = \cosh\left(\frac{q}{\kappa}\hat{P}\sqrt{12(1+1/\eta)}\right), \tag{A.8}$$

$$a_4 = \sinh(\lambda_0 \ell_B) = \sinh\left(\frac{(1-q)}{\kappa}\hat{P}\sqrt{12(1+1/\eta)}\right), \tag{A.9}$$

$$a_5 = \cosh(\lambda_0 \ell_B) = \cosh\left(\frac{(1-q)}{\kappa}\hat{P}\sqrt{12(1+1/\eta)}\right), \tag{A.10}$$

$$a_6 = \frac{1}{L\lambda_1} = \frac{q}{\lambda_1 \ell_A} = q\Big/\left(\frac{(1-q)}{\kappa}\hat{P}\sqrt{12(1+1/\eta)}\right), \tag{A.11}$$

and

$$a_7 = \frac{\lambda_0}{\lambda_1} = \frac{1}{a_2}. \tag{A.12}$$

With the help of Mathematica™ (Wolfram S., 1993), the unknown constants can be easily obtained and listed as follows.

*Case A. Clamped–clamped configuration*

$$\begin{aligned}\hat{M}_A = {} & (-(\alpha_n a_6 a_7) + \alpha_n a_3 a_4^2 a_6 a_7 + \alpha_n a_5 a_6 a_7 + \alpha_n a_3 a_5 a_6 a_7 - \alpha_n a_3 a_5^2 a_6 a_7 - \alpha_n a_4 a_7^2 \\ & + \alpha_n a_1 a_4 a_6 a_7^2)/(a_1 a_4 a_6 - a_1 a_5 a_7 - a_6 a_7 - a_1^2 a_4^2 a_6 a_7 + a_3^2 a_4^2 a_6 a_7 + 2a_3 a_5 a_6 a_7 \\ & + a_1^2 a_5^2 a_6 a_7 - a_3^2 a_5^2 a_6 a_7 - a_3 a_4 a_7^2 + a_1 a_4 a_6 a_7^2)\end{aligned} \tag{A.13}$$

$$\begin{aligned}\hat{R}_A = {} & (\alpha_n a_1 a_4 a_6 + \alpha_n a_1 a_4^2 a_7 - \alpha_n a_1 a_5^2 a_7 - \alpha_n a_6 a_7 - \alpha_n a_1^2 a_4^2 a_6 a_7 + \alpha_n a_3^2 a_4^2 a_6 a_7 + 2\alpha_n a_3 a_5 a_6 a_7 \\ & + \alpha_n a_1^2 a_5^2 a_6 a_7 - \alpha_n a_3^2 a_5^2 a_6 a_7 - \alpha_n a_4 a_7^2 + \alpha_n a_1 a_4 a_6 a_7^2)/(-(a_1 a_4 a_6) \\ & + a_1 a_5 a_7 + a_6 a_7 + a_1^2 a_4^2 a_6 a_7 - a_3^2 a_4^2 a_6 a_7 - 2a_3 a_5 a_6 a_7 - a_1^2 a_5^2 a_6 a_7 \\ & + a_3^2 a_5^2 a_6 a_7 + a_3 a_4 a_7^2 - a_1 a_4 a_6 a_7^2)\end{aligned} \tag{A.14}$$

$$A_1 = -\hat{M}_A \tag{A.15}$$

$$A_2 = (-(\alpha_n a_1 a_4 a_6) + \alpha_n a_1 a_5 a_7 + \alpha_n a_6 a_7 - \alpha_n a_3 a_6 a_7 - \alpha_n a_1^2 a_5 a_6 a_7 - \alpha_n a_3 a_5 a_6 a_7 + \alpha_n a_3^2 a_5 a_6 a_7)/(-(a_1 a_4 a_6) + a_1 a_5 a_7 + a_6 a_7 + a_1^2 a_4^2 a_6 a_7 - a_3^2 a_4^2 a_6 a_7 - 2a_3 a_5 a_6 a_7 - a_1^2 a_5^2 a_6 a_7 + a_3^2 a_5^2 a_6 a_7 + a_3 a_4 a_7^2 - a_1 a_4 a_6 a_7^2) \quad (A.16)$$

$$B_1 = -(a_n + \hat{R}_A)/a_6 \quad (A.17)$$

$$B_2 = (\alpha_n a_1 a_6 - \alpha_n a_1 a_5 a_6 + \alpha_n a_1 a_4 a_7 - \alpha_n a_1^2 a_4 a_6 a_7 - \alpha_n a_3 a_4 a_6 a_7 + \alpha_n a_3^2 a_4 a_6 a_7)/(a_1 a_4 a_6 - a_1 a_5 a_7 - a_6 a_7 - a_1^2 a_4^2 a_6 a_7 + a_3^2 a_4^2 a_6 a_7 + 2a_3 a_5 a_6 a_7 + a_1^2 a_5^2 a_6 a_7 - a_3^2 a_5^2 a_6 a_7 - a_3 a_4 a_7^2 + a_1 a_4 a_6 a_7^2) \quad (A.18)$$

*Case B. Roller–clamped configuration*

$$\hat{R}_A = (-(\alpha_n a_3 a_5^2) + \alpha_n a_2 a_3 a_4 a_6 + \alpha_n a_1 a_5 a_6 + \alpha_n a_2 a_3 a_4^2 a_7)/(a_3 a_5 - a_2 a_3 a_4 a_6 - a_1 a_5 a_6 + a_1 a_4 a_7) \quad (A.19)$$

$$A_1 = 0 \quad (A.20)$$

$$B_1 = (\alpha_n a_6 - \alpha_n a_5 a_6 + \alpha_n a_4 a_7)/(-(a_3 a_5) + a_2 a_3 a_4 a_6 + a_1 a_5 a_6 - a_1 a_4 a_7) \quad (A.21)$$

$$A_2 = (-(\alpha_n a_3 a_5) + \alpha_n a_1 a_6 + \alpha_n a_2 a_3 a_4 a_6)/(-(a_3 a_5) + a_2 a_3 a_4 a_6 + a_1 a_5 a_6 - a_1 a_4 a_7) \quad (A.22)$$

$$B_2 = B_1 a_2 a_3 \quad (A.23)$$

*Case C. Roller–roller configuration*

$$A_1 = 0, \quad (A.24)$$

$$B_1 = \frac{-\alpha_n a_5}{a_1 a_5 + a_2 a_3 a_4}, \quad (A.25)$$

$$A_2 = B_1 a_2 a_3, \quad (A.26)$$

$$B_2 = B_1 a_1 + \alpha_n. \quad (A.27)$$

## APPENDIX B

The following results are adapted from the literature on cracked lap shear specimens.

Table A.1. Case I (Johnson, 1987)

| | Young's modulus | Poisson's ratio | Thickness | Length |
|---|---|---|---|---|
| Strap (aluminum) | 72.45 GPa | 0.33 | 3.18 mm | 305 mm |
| Lap (aluminum) | 72.45 GPa | 0.33 | 3.18 mm | 254 mm |
| Adhesive | 1.932 GPa | 0.40 | 0.13 mm | |

This finite element analysis was performed by Dattaguru B. and Mangalgiri P. D. using GAMNAS program for the Round Robin compiled by Johnson (1987). Two dimensional, plane strain, and geometrical nonlinear options were used. The boundary conditions were equivalent to the roller-clamped case for the closed-form solution. The mode I, mode II, and total energy release rates were calculated based on a virtual crack extension method. The crack was assumed to lie at the center of the bondline.

Table A.2. Case II (Johnson, 1987)

| | Young's modulus | Poisson's ratio | Thickness | Length |
|---|---|---|---|---|
| Strap (aluminum) | 72.45 GPa | 0.33 | 3.18 mm | 305 mm |
| Lap (aluminum) | 72.45 GPa | 0.33 | 6.35 mm | 254 mm |
| Adhesive | 1.932 GPa | 0.40 | 0.13 mm | |

The method used in this case is the same as that in the Case I.

Table A.3. Case III (Dattaguru *et al.*, 1984)

| | Young's modulus | Poisson's ratio | Thickness | Length |
|---|---|---|---|---|
| Strap (aluminum) | 71.02 GPa | 0.33 | 3.2 mm | 254 mm |
| Lap (graphite/epoxy) | 130.93 GPa | 0.0188 | 1.6 mm | 203 mm |
| Adhesive | 4.14 GPa | 0.40 | N/A | |

This finite element analysis was performed using the GAMNAS program. Two dimensional, plane stress, and geometrical nonlinear options were used. The boundary conditions were equivalent to the roller–clamped case for the analytical solutions. The mode I, mode II, and total energy release rates were calculated based on a virtual crack extension method. The crack was assumed to lie at the center of the bondline.

Table A.4. Case IV (Mall and Yun, 1987)

| | Modulus | Poisson's ratio | Thickness | Length |
|---|---|---|---|---|
| Strap (graphite/epoxy) | 131* GPa | 0.34* | 2.0 mm | 241.3 mm |
| Lap (graphite/epoxy) | 131* GPa | 0.34* | 2.0 mm | 203.2 mm |
| Adhesive | 4.14** GPa | N/A | 0.2 mm | |

* Not listed in the paper, an estimated value for a unidirectional graphite/epoxy composite.
** Shear modulus.

How the finite element analysis was performed is not available in the paper. However, the plane strain analysis is assumed in the analytical solutions to compare with the results in this paper. The roller–clamped boundary conditions are used. The crack is assumed to be located at the center of the bondline.

Table A.5. Case V (Edde and Verreman, 1992)

| | Young's modulus | Poisson's ratio | Thickness | Length |
|---|---|---|---|---|
| Strap (aluminum) | 72 GPa | 0.33 | 3.2 mm | 250 mm |
| Lap (aluminum) | 72 GPa | 0.33 | 3.2 mm | 200 mm |
| Adhesive | 3.1 GPa | 0.41 | 0.3 mm | |

This finite element analysis was performed using the ABAQUS program. Two dimensional quadrilateral, plane strain element, and geometrical nonlinear options were used. The boundary conditions are equivalent to the clamped–clamped case for the analytical solutions. The mode I, mode II, and total energy release rates were calculated based on a modified virtual crack extension method. The crack was assumed to be located at the adhesive/strap interface.